Biomass Conversion and Biorefinery
https://doi.org/10.1007/s13399-022-03380-6

ORIGINAL ARTICLE

Isolation and characterization of cellulose nanocrystals from Chinese medicine residues

Qiang He[1] · Yu Bai[2] · Yuxi Lu[3] · Bo Cui[1] · Ziqiang Huang[1] · Qince Yang[1] · Donghua Jiang[1] · Dongwei Shao[1]

Received: 26 July 2022 / Revised: 19 September 2022 / Accepted: 9 October 2022

Abstract

Nanocellulose has become a vital material with excellent and crucial properties in the field of nanotechnology and advanced materials science. Plant-based traditional Chinese medicines are mostly plant rhizomes, which contain a large amount of cellulose, hemicellulose, and lignin. In this study, carboxylated cellulose nanocrystals (CNCs) were prepared from traditional Chinese medicine residues (CMR) by sequential periodate-chlorite oxidation without mechanical treatment. The obtained nanocelluloses were analyzed by transmission electron microscopy (TEM), Fourier transform infrared (FTIR) spectroscopy, thermogravimetric analysis (TGA), and X-ray diffractometry (XRD); the carboxyl content and specific surface area were also measured, simultaneously. XRD results revealed that the crystallinity index decreased after sequential oxidation; however, the cellulose I structure was maintained. From the morphology analysis, the average length and width of CNCs were 139.3 and 10 nm, respectively. From the FTIR analysis, with the particle size decreasing, hydrogen bonds were broken and recombined. TGA results showed that the thermal property was decreased with a reduction of nanocellulose particle size and crystallinity index. This study is the first to refine utilization of traditional Chinese medicine residues as a potential source of cellulose, that is, to prepare nanocellulose efficiently with high carboxyl content which finds its application in nanomaterials.

Keywords Chinese medicine residues · Purification · Periodate-chlorite · Nanocellulose

1 Introduction

Traditional Chinese medicine residues (CMRs) are mainly composed of herbal residues (such as plant roots, stems, leaves, flowers, etc.), nutrients, and minerals from animal sources. After the active ingredients extracted from the traditional Chinese medicine residues, the content of water is high. Moreover, there is still a large amount of cellulose, hemicellulose, lignin, a certain amount of protein, amino acids, polysaccharides and other active ingredients [1]. In the context of economic globalization, the traditional Chinese medicine industry has gradually integrated into the international pharmaceutical market. The annual discharge of medicinal residues has reached 70 million tons, of which about 70% are to be disposed, and the resources are relatively abundant [2]. Currently, in the face of the novel coronavirus pneumonia (Covid-19) pandemic, it had been shown that the use of traditional Chinese medicine had a positive effect. This further resulted in the production of a large amount of Chinese medicine residues [3, 4]. Traditional disposal methods such as stacking, incineration, and landfill lead to waste of resources and environmental pollution. Using a variety of treatment methods can give new economic value to the traditional Chinese medicine residues, so that the traditional Chinese medicine residues can be recycled or treated in a green and harmless manner. Deepika Singh et al. added Chinese medicinal residues to vermiculite, which improved the growth environment of earthworms. The number of beneficial bacteria in the soil is significantly increased, and the soil is rich in nutrients that can be used by plants [5]. Yang et al., designed a new alternative biosorbent that TiO_2-loaded biochar prepared by the Chinese traditional medicine residues were applied in remediation for As(III) from aqueous solution. The maximum adsorption capacity was 58.456 mg/g at 25 ℃ [6]. Traditional Chinese medicine residues can be

✉ Qiang He
heqiang4532@163.com

[1] College of Mechanical Engineering, Jiamusi University, Jiamusi 154007, Heilongjiang, China

[2] College of Engineering, Northeast Agricultural University, Harbin 150030, Heilongjiang, China

[3] Affiliated Hospital of Changchun University of Chinese Medicine, Changchun 130021, Jilin, China

Published online: 14 October 2022

transformed into bio-gas, bio-oil, biochar and other products with high economic value by pyrolysis [7].

Cellulose is a linear polysaccharide polymer composed of anhydroglucose and linked by β(1–4') glycosidic bonds. Nanocelluloses are a type of cellulosic materials with one-dimensional size in the nanoscale range. Nanocellulose can be mainly divided into short rod-like cellulose nanocrystals (CNCs), long fibrous cellulose nanofibers (CNFs), and bacterial nanocellulose (BNC) extracted from bacteria [8–10]. Nanocellulose has many special excellent properties, such as high specific surface area, high mechanical strength, high purity, and high adsorption, etc. There are many active groups on its surface, which can be chemically modified to obtain excellent performance, derived various cellulose nanofunctional materials [11–13].

Cellulose nanocrystals was first successfully prepared by Nickerson and Habrle in 1947 by hydrolysis of cellulose with hydrochloric and sulfuric acid [14]. In 1950s, Mukherjee SM prepared stable cellulose nanocrystals colloidal suspensions by hydrolyzing wood fibers with sulfuric acid. The cellulose nanocrystals prepared by acid hydrolysis can form birefringent gels and liquid crystal structures, and exhibit helical self-ordering (chiral nematic phase) properties within a certain concentration range [15, 16]. Liu et al. reported the use of bleached pulp and solid phosphotungstic acid ($H_3PW_{12}O_{40}$) hydrolysis to prepare cellulose nanoparticles with diameters of 15–40 nm and lengths of hundreds of nanometers, which possessed superior thermodynamic properties [17]. The advantages of solid acid hydrolysis to prepare nanocellulose were that the acid was easy to recover and had low corrosiveness. At the same time, the disadvantages are high cost of solid acid, long hydrolysis time, low yield, inhomogeneity of the hydrolysis process, and wide particle size distribution. Vidhi et al. proposes valorization of amla (Phyllanthus emblica) pomace for the isolation of cellulose nanocrystals [18]. Suman et al. isolated cellulose nanocrystals from seaweed by microwave-assisted alkali treatment, bleaching, and an acid hydrolysis process [19].

The short rod-shaped cellulose nanocrystals were used in reinforcing fillers, template materials, etc. It has the unique advantage of one-dimensional rod-shaped morphology in addition to the order of the crystalline structure [20]. The cellulose nanocrystals modified by surface functionalization have derived a wide range of applications. He et al. prepared dicarboxyl cellulose nanocrystals from spent edible fungus substrates of which adsorped the amoxicillin (9.63 mg/g) [21]. Sun et al. reported the nanocellulose with rich carboxyl groups was prepared through the sequential oxidation method to efficiently remove copper ions (184.2 mg/g) [22]. Sun et al. developed a simple, rapid, and accurate Fe^{3+} detection method. Fluorescent dicarboxylic cellulose nanocrystals with selective quenching of Fe^{3+} were synthesized using 7-amino-4-methylcoumarin. High sensitivity with a detection limit of 0.26 mM and a Stern–Volmer quenching constant of 0.1229 were achieved [23]. Xu et al. designed an optimal carboxylated cellulose nanocrystals-producing left-handed chiral nematic films by evaporation-induced self-assembly are obtained with tuning the aspect ratio and surface charge density [24]. Cellulose and its derivatives have been extensively used for delivering growth factors and antibiotics directly to the site of the impaired bone tissue to promote tissue repair [25]. Bacterial nanocellulose scaffolds were implanted in different bone defects created in the tibia, calvarial bones, and skull in rats and promoted new bone formation without any inflammatory reactions [26]. Reinforcing the GEL/BG scaffold with CNCs led to improved compressive strength, wettability, and favorable adhesion and proliferation of cells [27].

Currently, the raw materials for preparing nanocellulose are mainly cotton, wood, and straw, etc.. To achieve a circular economy of resources, cellulose sources should be diverted to non-food crops or process wastes. As a renewable resource with huge annual output, traditional Chinese medicine residue can be used as a new source of cellulose to prepare nanocellulose. The acid hydrolysis process was relatively mature, but the reaction would produce a large amount of acidic waste liquid and impurities, which required high corrosion resistance of the equipment, and nanocellulose was also difficult to collect, and a large amount of water need to be consumed in the cleaning process. As a result, it is mainly used for laboratory research at present, and further improvement is required for industrial production. Therefore, our study aimed to produce high quantities of carboxylated cellulose nanocrystals with high content functional groups from traditional Chinese medicine residues by sequential periodate-chlorite without mechanical process while investigating the chemical, morphological, and thermal properties of the obtained cellulose.

2 Materials and methods

2.1 Materials

Never-dried Chinese medicine residues (CMR) were supplied by the Affiliated Hospital of Changchun University of Traditional Chinese Medicine. All chemicals were purchased from Damao Fine Chemical Co., Ltd. (Tianjin China) and used without further purification (analytical grade). Deionized water was used throughout the experiments.

2.2 Methods

2.2.1 Pre-treatment of Chinese medicine residues

Celluloses from Chinese medicine residues (CMRs) were extracted by bleaching and alkalizing methods at room temperature. Chinese medicine residues were soaked in water

for 48 h prior to any chemical treatment. Bleaching was performed for 2 h with $NaClO_2$ (being adjusted to pH = 4 with CH_3COOH) at a ratio of 1:50 (w/v) using stirring. The obtained fibers were dispersed into 1L NaOH of 2.5%/5% for 2 h at 90 °C consecutively. Finally, the second bleaching was performed for 6 h with $NaClO_2$ (being adjusted to the pH = 4 with CH_3COOH) at a ratio of 1:50 (w/v) using stirring. The recovered fibers (named CMR1-CEL/CMR2-CEL) were washed thoroughly with deionized water until reaching neutral pH and oven-dried to a constant mass [21, 28].

2.2.2 Isolation of cellulose nanocrystals

Periodate oxidation was performed as previously described with minor changes. Typically, 4 g of cellulose was soaked in water (250 mL) for 24 h at room temperature, next added 5.33 g $NaIO_4$, 15.6 g NaCl. Meanwhile, the beaker was wrapped with several layers of aluminum foils to prevent entry of any light, and the reaction was performed and stirred for 24 h. The oxidized fibers (dialdehyde cellulose) were thoroughly washed with deionized water by centrifugal (3000 g for 5 min, Allegra V-15R, Beckman Coulter International Trading (Shanghai) Co., Ltd.) until the conductivity of the supernatant was less than 30 µS/cm. The DACs were dried in a vacuum freeze-dryer [21, 29].

One gram of dialdehyde cellulose was suspended in 50 mL water, 2.93 g of NaCl, $NaClO_2$, and H_2O_2 (with molarity twice that of the aldehyde content of the DAC) were added into the mixture with stirring for 24 h at room temperature. and the pH value was maintained at 5 by adding 0.5 M NaOH. After the reaction completed, the final products (cellulose nanocrystals, named CMR1-CNC/CMR2-CNC) were washed by centrifugal with 0.1 M NaOH for three times and then with deionized water for several times until the conductivity of the supernatant was less than 30 µS/cm, then stored at 4 °C [30].

2.2.3 Chemical compositions

Compositional analyses of CMR and CMR-CEL were performed with the ANKOM A200i semi-automatic fiber analyzer, which can determine the substance composition by measuring neutral detergent fiber (NDF), acid detergent fiber (ADF), and acid detergent lignin (ADL).

2.2.4 X-ray diffraction (XRD)

The crystalline structure was performed on an X-ray diffractometer (D/MAX2200VPC, Rigaku Corporation, Japan) using Cu$K\alpha$ radiation ($\lambda = 0.154$ nm) at 40 kV and 40 mA. Diffraction data was collected in the range of $2\theta = 5$–40°, at a scanning rate of 0.5°/min. The relative crystallinity index (*CrI*) was calculated using the Segal method with the following Eq. 1:

$$CrI(\%) = \frac{I_{002} - I_{am}}{I_{002}} \times 100\% \quad (1)$$

I_{002} and I_{am} are the maximum diffraction intensity at a diffraction angle of 22–23° and the minimum diffraction intensity at a diffraction angle of 18–20°.

2.2.5 Fourier transform infrared (FTIR) spectroscopy

The Fourier transform infrared (FTIR) spectroscopy spectra were recorded over the 500–4000 cm^{-1} range in transmittance mode with 32 scans at a resolution of 4 cm^{-1} using an infrared spectrometer instrument (IRTracer-100, Shimaduz Ltd., Kyoto Japan). The background was subtracted prior to the analysis.

2.2.6 TEM particle size

The morphology was observed with the transmission electron microscopy (TEM) using a JEM-2100 transmission electron microscope (JEOL Ltd, Japan) at an accelerator voltage of 200 kV. The dimensions of the CNCs were calculated from the TEM images using the Image J software. According to the hypothetical nanocellulose cylinder model, the specific surface area was calculated by the following Eq. 2:

$$\text{Specific surface area } \left(SSA, \mathrm{m}^2/g\right) = \frac{4}{\rho \bullet d} \quad (2)$$

where ρ is the density of cellulose (1.5 g/cm^3) and d is the diameter of a single CNC.

2.2.7 Aldehyde content

The aldehyde content was determined by an oxime reaction through titration. A 0.1 g DAC, 10 ml of water, and 20 ml of isopropanol were mixed and stirred for 0.5 h. Next, the concentrated HCl was added dropwise to adjust the pH of the mixture to 2–3, following the pH was adjusted to 3.5 with 0.1 M NaOH. Then, 10 mL of a 10% NH_2OH-HCl was added to the mixture and allowed to react for 30 min. Finally, the solution was titrated with a 0.5 mol/L NaOH solution until the pH reached 3.5. The aldehyde content was calculated with the following Eq. 3:

$$C_{-\mathrm{CHO}} = \frac{V_{\mathrm{NaOH}} \times N}{W_{\mathrm{cellulose}}} \quad (3)$$

where C_{-CHO} is the content of aldehyde group (mmol/g cellulose); V_{NaOH} is the volume of NaOH (mL); N is the NaOH

equivalent concentration (0.5 mol/L); and $W_{cellulose}$ is the weight of initially suspended DAC (g).

2.2.8 Conductometric titration

CNC (0.1 g) was mixed with 100 ml 0.5 M NaCl aqueous solution and stirred evenly, then add 5 ml 0.1 M HCl-0.5 M NaCl mixed solution. Titration with a mixture of 0.1 M NaOH-0.5 M NaCl with stirring. Automatic potentiometric titrator records potential changes throughout the reaction (ZD-2, Shanghai LeiCi Magnetic Instrument Co., Ltd., China). After the reaction was completed, a graph of NaOH consumption compared to $\Delta E^2/\Delta V^2$ was made according to the two-stage differential methods. The inflection point of the curve was the total NaOH consumption during the reaction, and then the NaOH consumption of the carboxyl group was determined, and three parallel experiments were performed.

$$C_{-COOH} = \frac{\left(V_{NaOH} - V_{HCl}\right) \times M_{NaOH}}{W_{cellulose}} \quad (4)$$

where C_{-COOH} is the carboxyl content (mmol/g), V_{NaOH} is the volume of NaOH at the inflection point (ml), V_{HCl} is the volume of HCl added to the 0.1 M HCl-0.5 M NaCl mixed solution (mL); M_{NaOH} is equivalent concentration of NaOH (mol/L), and $W_{cellulose}$ is the starting mass of CNCs (g).

2.2.9 Thermogravimetric analysis

The thermal stability was tested by thermal gravimetric analysis (METTLER TOLEDO, SDTA851e, Switzerland) at a heating rate of 10 °C/min from 50 to 600 °C under a nitrogen atmosphere (25 ml/min).

3 Results and discussion

3.1 Composition and yield analysis

The chemical constituents of Chinese medicine residues were measured by the VanSoest method. As shown in Table 1, the cellulose average content (mass fraction) in the traditional Chinese medicine residue was 33.36%, the hemicellulose content was 17.78%, the lignin content was 10.32%, and the others (starch, pectin, protein, etc.) account for 38.57%. Consistent with the cellulose content of other common agricultural and forestry wastes (32.25% for spent edible fungus substrate, 38.04% for rice straw, 35.66% for corn straw) [21, 31, 32].

The traditional Chinese medicine residues were treated with acidic sodium chlorite and gradient alkali solution. In the reaction process of acidic sodium chlorite, the oxidation reaction played a leading role. At the same time, water molecules have a moisturizing effect on cellulose, which effectively moistens and swells the inner space of fibers, promotes fiber separation, and facilitates subsequent alkaline solution gradient treatment [33]. Then, the potassium hydroxide alkaline solution was subjected to gradient treatment; the color of the solution changed to dark brown; obviously, the straw solid was light brown, and a large amount of lignin and hemicellulose were dissolved in the alkaline solution, and the gradient concentration treatment adopted two consecutive alkaline solution treatments to further increase fiber content [34]. Next, the obtained fibers were re-bleached with acid sodium chlorite. The oxidative properties of acid sodium chlorite can oxidize the benzene ring and double-bond structure in the lignin molecule, thereby decomposing the lignin in the traditional Chinese medicine residues. Finally, purified cellulose was obtained by filtration.

3.2 X-ray diffraction

The crystal structure and Crystallinity Index of nanocellulose were analyzed by X-ray diffraction pattern. Typical peaks for cellulose were shown by Nishiyama and Isogai et al., with 2θ angles of 15.3°, 16.3°, and 22.6°, corresponding to the ($\bar{1}$10), (110) and (200) peaks [35, 36]. The XRD diffraction pattern of purified celluloses from the traditional Chinese medicine residues (CMR1-CEL, CMR2-CEL) had typical peaks of type I cellulose [37]. It can be seen from Fig. 1 that the purification treatment does not destroy the crystal structure of cellulose. After calculation, the crystallinity index of purified celluloses were 74.1% and 76.4%, respectively, which was lower than that of commercial production of 83.91% (Microcrystalline cellulose, Shanghai Sinopharm Reagent Co., Ltd.). The cyclic treatment of sodium chlorite and potassium hydroxide in the purification process resulted in a slightly lower crystallinity index of the purified cellulose (CMR1-CEL, CMR2-CEL). However, the

Table 1 Chemical composition of various cellulose samples

	CMR1	CMR2	CMR1-CEL	CMR2-CEL
Cellulose (%)	32.15 ± 0.36	34.56 ± 0.17	96.15 ± 0.18	97.22 ± 0.20
Hemicellulose (%)	17.44 ± 0.03	18.09 ± 0.32	1.23 ± 0.33	0.91 ± 0.54
Lignin (%)	9.92 ± 0.87	10.71 ± 0.78	0.76 ± 1.02	0.88 ± 0.17
Others (%)	40.49 ± 0.22	36.64 ± 0.71	1.86 ± 0.92	0.99 ± 0.31

decrease of crystallinity was favorable for the subsequent oxidation of sodium periodate and sodium chlorite. At the same time, the crystal form of cellulose nanocrystals had not changed, and it was still the cellulose I-type structure, and the typical peaks of Iβ cellulose were preserved.

The calculation showed that the CrI of the nanocellulose (CMR1-CNC, CMR2-CNC) obtained by the sequential oxidation of $NaIO_4$-$NaClO_2$ was 65.8% and 61.5%, respectively. This result was consistent with experiments conducted by Varma et al. and Kim et al. [38, 39]. They found that the crystallinity index of cellulose decreased as the degree of oxidation of periodate and chlorite increased. Cellulose was a typical chain compound containing a crystalline region and an amorphous region, which led to significant differences in the sensitivity and accessibility of chemical reagents in different regions. It can be seen from theoretical analysis that in the process of the reaction between cellulose and $NaIO_4$, firstly, the oxidant molecule reacted with the highly active non-crystalline region, where hydrolysis and elimination reactions occurred, and severe side reactions led to chain scission of cellulose. So that the crystallinity index of nanocellulose crystals decreased slightly.

3.3 FTIR analysis

Chemical structural characterization of cellulosic fibers was performed using FTIR to identify functional groups present in each sample. As shown in Fig. 2, the broad absorption peak at 3350 cm^{-1} was caused by the stretching vibration of hydroxyl (–OH) in cellulose. It was proposed that the structure of cellulose I is that the molecular chains are stacked according to parallel chains, and the molecules existing in the molecular chain Inter-hydrogen bonding is the main factor responsible for this absorption peak [40, 41]. 2914 cm^{-1} was the C–H stretching vibration peak of methyl, methylene, and methine. The prominent peak at 1730 cm^{-1} was not visible in the purified cellulose of traditional Chinese medicine residues (CMR1-CEL, CMR2-CEL), indicating that there was no ester bond of lignin or hemicellulose carboxyl, acetyl groups, or sugar of hemicellulose. Due to the vibration of adsorbed water molecules, there was an absorption peak at 1640 cm^{-1}, indicating that cellulose and water had a strong interaction, and it was difficult to completely dry. The absorption peak at 1436 cm^{-1} was the bending vibration associated with $–CH_2$ and O–CH. The absorption peak

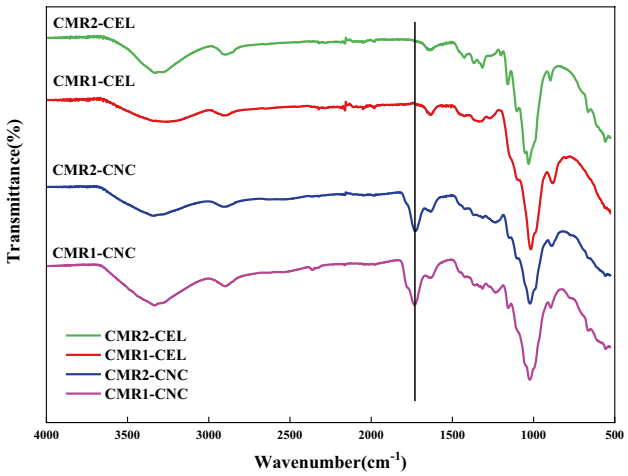

Fig. 2 FTIR spectra recorded between 4000 and 500 cm^{-1} of purified cellulose and CNCs

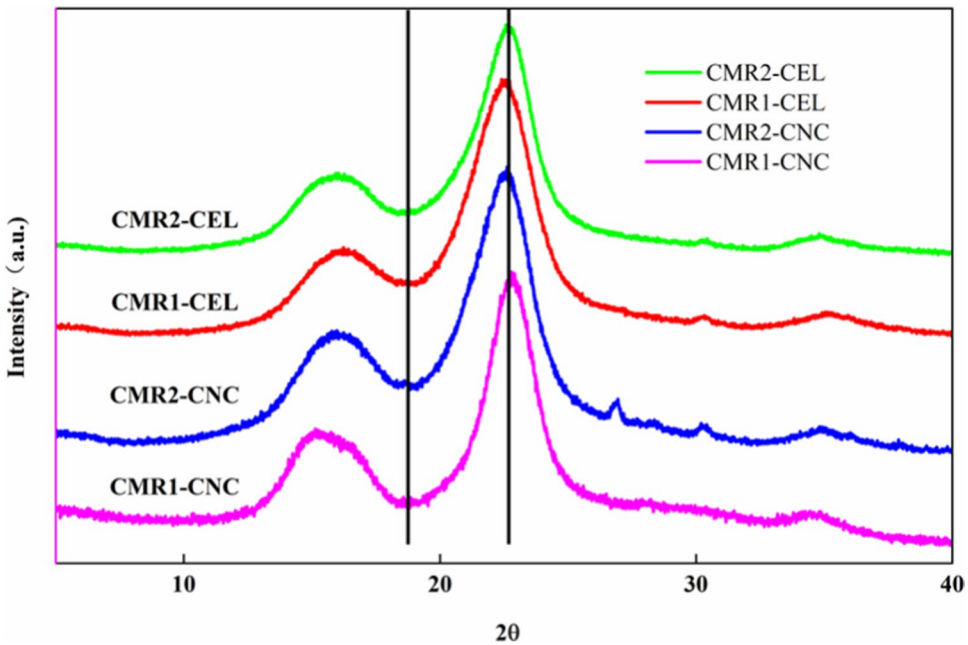

Fig. 1 XRD patterns of purified celluloses and CNCs

at 1167 cm^{-1} corresponds to the stretching vibration of the C–O group, and the absorption peak at 1030 cm^{-1} corresponds to the asymmetric stretching vibration of C_1–O–C_4 in the glucopyranose ring [42].

The absorption peak at 893 cm^{-1} was a characteristic structural peak of cellulose, which represented the β-glycosidic linkage of the glucose ring. It can be seen from the analysis that the increase in the intensity of the absorption peak at 893 cm^{-1} indicated that the purified cellulose had been improved in the process of preparing MCC with traditional Chinese medicine residues which was consistent with the XRD results [43]. The peak shapes of the samples were similar, indicating that the cellulose did not undergo derivatization during the purification process of the traditional Chinese medicine residue, and still had a typical cellulose I structure. For CMR1-CNC and CMR2-CNC, the carboxy groups in the solid nanocellulose crystals exist in the form of dimers, and the –O–H stretching vibration occurs at 3300 cm^{-1}, and due to the hydrogen bond, the absorption peak of C = O shifted to 1720 cm^{-1} to the low frequency end, which proved that the hydroxyl group on the cellulose molecule had been successfully oxidized to the carboxyl group [44].

3.4 Morphological and functional group content analysis

First, it can be clearly observed from Fig. 3a, b that the scale of CMR-CNCs reached the nanometer level. According to the literature, periodate attacked the non-crystalline region on the cellulose chain, and the non-crystalline region was gradually hydrolyzed to obtain a crystalline region with high crystallinity and a part of the residual non-crystalline region, resulting in an intermediate product of dialdehyde cellulose (DAC). Sodium chlorite oxidized the aldehyde groups on the surface of the DAC to the carboxyl groups, and the negative charge of the carboxyl groups increased the electrostatic repulsion between the cellulose chains, thus releasing nano-scale carboxylated cellulose nanocrystals. The average carboxyl content of CMR1-CNC and CMR2-CNC measured by conductometric titration was 3.21 mmol/g, respectively. Compared with the Tempo-NaBr-NaClO method, that oxidized the hydroxyl of the C-6 position, the nanocellulose prepared by our study oxidized the hydroxyl of the C-2,3 positions and had a larger content of active functional groups, which provided more possibilities for the subsequent graft modification of nanocellulose [30]. In addition, it can be seen that the cellulose of CNCs was in the shape of short rods, which were thin at the ends and thick in the middle. According to the literature, the accessibility of the amorphous region of cellulose is high, and the oxidation reaction was first carried out in the amorphous region, and then entered the crystalline region. And the rate of periodate oxidation at the end of the crystal was about 10 times higher than that at the side of the crystal, resulting in cellulose nanocrystals exhibiting a short rod-like morphology with thicker middle and thinner ends [45]. Finally, the particle size distribution histogram was shown in the Fig. 4. As shown in Table 2, according to the average statistical results of 200 cellulose fibers under the transmission electron microscope, the average particle size of the prepared CNC is 10 nm, the average length is 139.3 nm, and the calculated DNC aspect ratio was 14.19, and the specific surface area was 269.5 m^2/g and had great advantages compared with other preparation methods. Therefore, through preliminary TEM analysis, the nanostructure and high specific surface area of CNC can provide many possibilities for other applications [46].

3.5 Thermal analysis

Thermogravimetric analysis was performed for CMR-CELs and CMR-CNCs. The TGA and differential thermogravimetry (DTG) curves for nanocelluloses and purified celluloses were shown in Fig. 5, respectively. The initial weight loss (10%) in the temperature range of 50–235 °C may be attributed to the evaporation of water molecules present in the samples. The second stage was the thermal

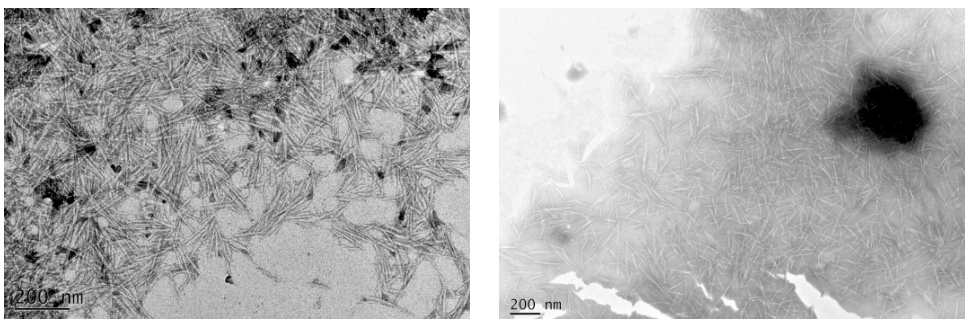

(a) (b)

Fig. 3 TEM images of CMR1-CNC (**a**) and CMR2-CNC (**b**)

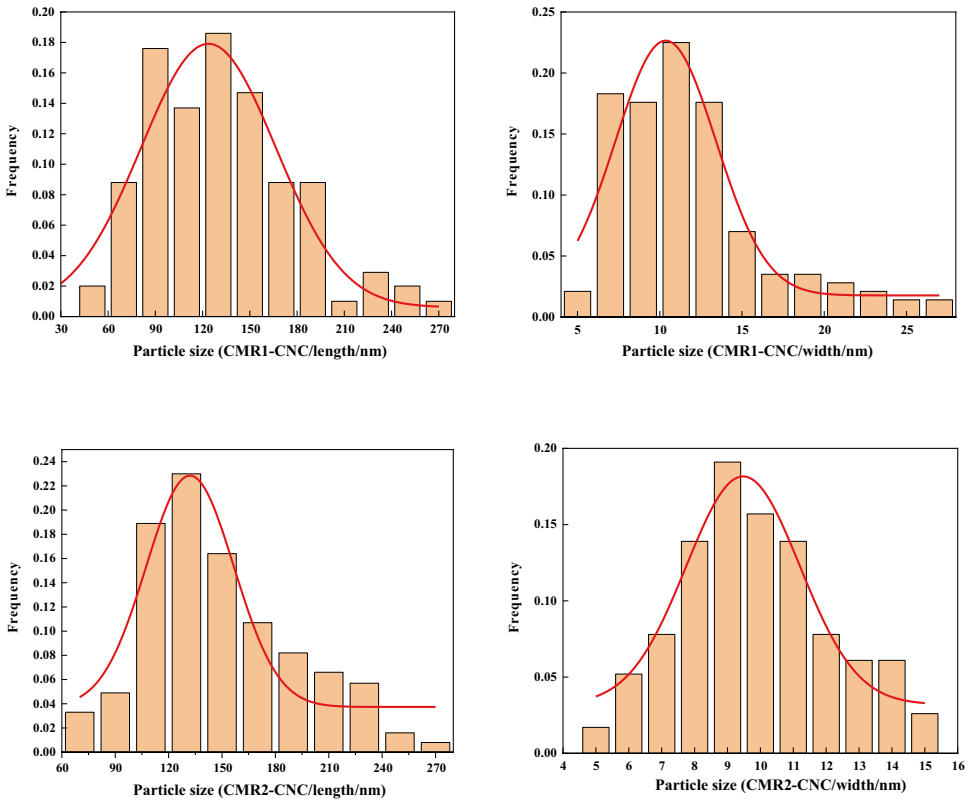

Fig. 4 Particle size distribution curve of CMR1-CNC and CMR2-CNC

Table 2 Morphology characteristics of CNCs

	CMR1-CNC	CMR2-CNC
Carboxyl (mmol/g)	3.15 ± 0.29	3.27 ± 0.17
Length (nm)	131.6 ± 46	147.0 ± 44
Width (nm)	11.1 ± 3.8	8.9 ± 2
L/W	11.86	16.52
SSA (m^2/g)	240	299

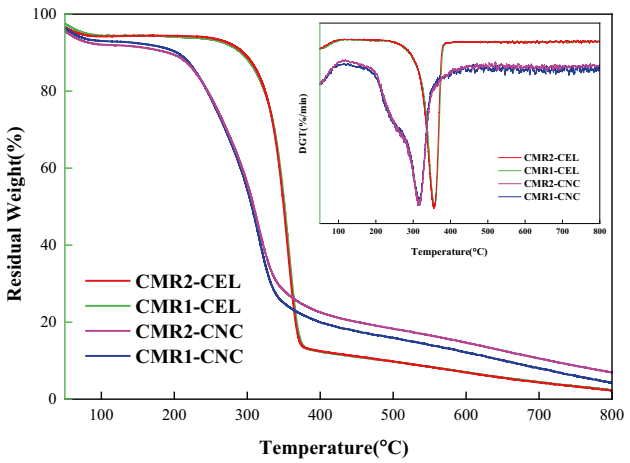

Fig. 5 TGA curves of purified cellulose (CEL) and CNCs

degradation stage of nanocellulose crystals from 235 to 313 °C. It showed that the non-cellulose components and the cellulose amorphous area were effectively removed after the purification treatment of the traditional Chinese medicine residue [47]. The mass loss in this area was approximately 68%. As the temperature further increased, the nanocellulose crystals began to undergo thermal degradation, accompanied by a decrease in the mass percentage of solid residues, and the formation of CO_2, H_2O, CO, and solid coke residues were detected. As can be seen from the DSC curve, the pyrolysis temperature of the isolated Chinese medicine residue cellulose through sodium chlorite and alkalization treatment reached 333 °C. Compared with the extracted nanocellulose, the thermal decomposition onset temperature was reduced by about 98 °C. This was attributed to the substitution of carboxylic acid groups for the meridian groups on the surface of CNC, which accelerated the degradation reaction of CNC, which was also confirmed by TGA [48]. The temperature range of the third stage was 316 to 800 °C, and in the stage above 500 °C, the final solid residue is 16%. The thermal stability of cellulose was better than that of CNCs in the low temperature region, and the final mass residue were 16% and 23% for the CMR-CEL and the CMR-CNC, respectively. This phenomenon can be attributed to the fact that the surface of the CNC possessed a large number of

carboxyl groups, which had better cross-linking properties, resulting in better thermal resistance at high temperatures.

4 Conclusions

In this study, traditional Chinese medicine residues were found as a new source of cellulose, which had been utilized for the extraction of cellulose and preparation of nanocellulose. Purified celluloses were successfully extracted from traditional Chinese medicine residues after alkali treatment followed by bleaching. Composition analysis and FTIR study revealed the partial removal of hemicellulose and lignin after pre-treatment. Cellulose nanocrystals were prepared with sequential periodate-chlorite oxidation without mechanical process resulting in rod-like CNCs with an average length of 139.3 nm and width of 10 nm. Compared with the purified cellulose from traditional Chinese medicine residues, the TGA results showed that the thermal stability of nanocellulose crystals decreased, which could be attributed to the decrease in particle size and the increase in specific surface area. This result was further confirmed by XRD analysis of the two samples that the crystallinity index of cellulose decreased as the degree of oxidation of periodate and chlorite increased. This study establishes the fact that traditional Chinese medicine residues has an enormous potential as a source for high carboxyl content cellulose nanocrystals which finds its application in material science and composite making. At the same time, the theory of cellulose extraction can be shifted to a chlorine-free process, and other agricultural and food industry wastes can also be considered as cellulose sources.

Acknowledgements The authors would like to thank the College of Engineering, Northeast Agricultural University, for providing the laboratory and material testing. Special thanks to Yuxi Lu for providing the raw materials of traditional Chinese medicine residues used in the experiment.

Author contribution Qiang He and Yuxi Lu took the lead in preparing the manuscript and carrying out the experiments. Qiang He, Yu Bai, and Bo Cui contributed in conceiving and planning the experiments. Ziqiang Huang and Qince Yang helped with the analysis part. Donghua Jiang and Dongwei Shao contributed to the interpretation of the results. All authors provided critical feedback and helped shape the research, analysis, and manuscript.

Funding This research was funded by Heilongjiang Provincial Department of Education and Jiamusi University. The authors would like to acknowledge the support of the basic scientific research funds project of Heilongjiang Universities (grant number: 2021-KYYWF-0560).

Data availability The datasets used and/or analyzed during the current study are available from the corresponding author on reasonable request.

Declarations

Ethics approval Not applicable.

Consent for publication Not applicable.

Competing interests The authors declare no competing interests.

References

1. Lu Q, Li C (2021) Comprehensive utilization of Chinese medicine residues for industry and environment protection: turning waste into treasure. J Clean Prod 279:123856. https://doi.org/10.1016/j.jclepro.2020.123856
2. Gao R-R, Hu Y-T, Dan Y, Hao L-J, Liu X, Song J-Y (2020) Chinese herbal medicine resources: where we stand. Chin Herb Med 12(1):3–13. https://doi.org/10.1016/j.chmed.2019.08.004
3. Shu Z, Zhou Y, Chang K, Liu J, Min X, Zhang Q, Sun J, Xiong Y, Zou Q, Zheng Q, Ji J, Poon J, Liu B, Zhou X, Li X (2020) Clinical features and the traditional Chinese medicine therapeutic characteristics of 293 COVID-19 inpatient cases. Front Med 14(6):760–775. https://doi.org/10.1007/s11684-020-0803-8
4. Lyu M, Fan G, Xiao G, Wang T, Xu D, Gao J, Ge S, Li Q, Ma Y, Zhang H, Wang J, Cui Y, Zhang J, Zhu Y, Zhang B (2021) Traditional Chinese medicine in COVID-19. Acta Pharm Sin B 11(11):3337–3363. https://doi.org/10.1016/j.apsb.2021.09.008
5. Singh D, Suthar S (2012) Vermicomposting of herbal pharmaceutical industry waste: earthworm growth, plant-available nutrient and microbial quality of end materials. Bioresour Technol 112:179–185. https://doi.org/10.1016/j.biortech.2012.02.101
6. Yang Y, Zhang R, Chen S, Zhu J, Wu P, Huang J, Qi S (2022) Arsenic(iii) removal from aqueous solution using TiO2-loaded biochar prepared by waste Chinese traditional medicine dregs. RSC Adv 12(13):7720–7734. https://doi.org/10.1039/D1RA08941B
7. Liang F, Wang R, Hongzhong X, Yang X, Zhang T, Hu W, Mi B, Liu Z (2018) Investigating pyrolysis characteristics of moso bamboo through TG-FTIR and Py-GC/MS. Bioresour Technol 256:53–60. https://doi.org/10.1016/j.biortech.2018.01.140
8. Norfarhana AS, Ilyas RA, Ngadi N (2022) A review of nanocellulose adsorptive membrane as multifunctional wastewater treatment. Carbohydr Polym 291:119563. https://doi.org/10.1016/j.carbpol.2022.119563
9. Dhali K, Ghasemlou M, Daver F, Cass P, Adhikari B (2021) A review of nanocellulose as a new material towards environmental sustainability. Sci Total Environ 775:145871. https://doi.org/10.1016/j.scitotenv.2021.145871
10. Choudhury RR, Sahoo SK, Gohil JM (2020) Potential of bioinspired cellulose nanomaterials and nanocomposite membranes thereof for water treatment and fuel cell applications. Cellulose 27(12):6719–6746. https://doi.org/10.1007/s10570-020-03253-z
11. Liu Y, Liu A, Ibrahim SA, Yang H, Huang W (2018) Isolation and characterization of microcrystalline cellulose from pomelo peel. Int J Biol Macromol 111:717–721. https://doi.org/10.1016/j.ijbiomac.2018.01.098
12. Mateo S, Peinado S, Morillas-Gutiérrez F, La Rubia MD, Moya AJ (2021) Nanocellulose from agricultural wastes: products and applications—a review. Processes 9(9). https://doi.org/10.3390/pr9091594
13. Gupta V, Yadav R, Tanwar R, Gaikwad KK (2021) κ-Carrageenan-based bio-nanocomposite film reinforced with cellulose nanocrystals derived from amla pomace for food packaging. Biomass Convers Biorefin. https://doi.org/10.1007/S13399-021-02028-1

14. Nickerson RF, Habrle JA (1947) Cellulose intercrystalline structure. Ind Eng Chem 39(11):1507–1512. https://doi.org/10.1021/ie50455a024
15. Revol JF, Bradford H, Giasson J, Marchessault RH, Gray DG (1992) Helicoidal self-ordering of cellulose microfibrils in aqueous suspension. Int J Biol Macromol 14(3):170–172. https://doi.org/10.1016/S0141-8130(05)80008-X
16. Mukherjee SM, Woods HJ (1953) X-ray and electron microscope studies of the degradation of cellulose by sulphuric acid. Biochim Biophys Acta 10:499–511. https://doi.org/10.1016/0006-3002(53)90295-9
17. Liu Y, Wang H, Yu G, Yu Q, Li B, Mu X (2014) A novel approach for the preparation of nanocrystalline cellulose by using phosphotungstic acid. Carbohydr Polym 110:415–422. https://doi.org/10.1016/j.carbpol.2014.04.040
18. Gupta V, Ramakanth D, Verma C, Maji PK, Gaikwad KK (2021) Isolation and characterization of cellulose nanocrystals from amla (Phyllanthus emblica) pomace. Biomass Convers Biorefin. https://doi.org/10.1007/s13399-021-01852-9
19. Singh S, Gaikwad KK, Park S-I, Lee YS (2017) Microwave-assisted step reduced extraction of seaweed (Gelidiella aceroso) cellulose nanocrystals. Int J Biol Macromol 99:506–510. https://doi.org/10.1016/j.ijbiomac.2017.03.004
20. Wang Y, Xie R, Li D, Shen Y, Xie W, Wang H, Gan L, Huang J (2020) A cross-linking/percolating-integrated strategy to enhance crystallizable rubber using rod-like reactive biobased nanocrystals. ACS Appl Bio Mater 3(1):441–449. https://doi.org/10.1021/acsabm.9b00901
21. He Q, Yang Y, Liu Z, Shao D, Jiang D, Xing L, Pan Q, Shan H (2022) Preparation and characterization of cellulose nanocrystals from spent edible fungus substrate. J Sci Food Agric 102(7):2761–2772. https://doi.org/10.1002/jsfa.11617
22. Sun X, Yang Y, He Q, Li J, Li R, Chen H (2022) Adsorption properties and cost of dicarboxylic nanocellulose on copper ions for wastewater treatment. J Renew Mater 10(3). https://doi.org/10.32604/jrm.2022.016933
23. Sun X, Li J, He Q, Xue Y, Bai Y, Yang Y, Wang X, Wang S, Li R (2022) Ferric ion detection mechanism of a dicarboxylic cellulose nanocrystal and a 7-amino-4-methylcoumarin based fluorescent chemosensor. RSC Adv 12(26):16798–16804. https://doi.org/10.1039/D2RA02303B
24. Fan W, Li J, Wei L, Xu Y (2022) Carboxylated cellulose nanocrystal films with tunable chiroptical properties. Carbohydr Polym 289:119442. https://doi.org/10.1016/j.carbpol.2022.119442
25. Janmohammadi M, Nazemi Z, Salehi AOM, Seyfoori A, John JV, Nourbakhsh MS, Akbari M (2023) Cellulose-based composite scaffolds for bone tissue engineering and localized drug delivery. Bioact Mater 20:137–163. https://doi.org/10.1016/j.bioactmat.2022.05.018
26. Torgbo S, Sukyai P (2018) Bacterial cellulose-based scaffold materials for bone tissue engineering. Appl Mater Today 11:34–49. https://doi.org/10.1016/j.apmt.2018.01.004
27. Gao W, Sun L, Zhang Z, Li Z (2020) Cellulose nanocrystals reinforced gelatin/bioactive glass nanocomposite scaffolds for potential application in bone regeneration. J Biomater Sci Polym Ed 31(8):984–998. https://doi.org/10.1080/09205063.2020.1735607
28. Kumar A, Gupta V, Gaikwad KK (2021) Microfibrillated cellulose from pine cone: extraction, properties, and characterization. Biomass Convers Biorefin. https://doi.org/10.1007/s13399-021-01794-2
29. Chen D, van de Ven TGM (2016) Morphological changes of sterically stabilized nanocrystalline cellulose after periodate oxidation. Cellulose 23(2):1051–1059. https://doi.org/10.1007/s10570-016-0862-9
30. Yang H, Alam MN, van de Ven TGM (2013) Highly charged nanocrystalline cellulose and dicarboxylated cellulose from periodate and chlorite oxidized cellulose fibers. Cellulose 20(4):1865–1875. https://doi.org/10.1007/s10570-013-9966-7
31. Wang L, Li Y, Xu L, Sun D, Wang Y, Wang Z (2022) Rice straw pretreatment using cow breeding wastewater for methane production. Bioresour Technol 346:126657. https://doi.org/10.1016/j.biortech.2021.126657
32. Jin Y, Zhang B, Chen G, Chen H, Tang S (2022) Combining biological and chemical methods to disassemble of cellulose from corn straw for the preparation of porous carbons with enhanced adsorption performance. Int J Biol Macromol 209:315–329. https://doi.org/10.1016/j.ijbiomac.2022.04.033
33. Okugawa A, Sakaino M, Yuguchi Y, Yamane C (2020) Relaxation phenomenon and swelling behavior of regenerated cellulose fibers affected by water. Carbohydr Polym 231:115663. https://doi.org/10.1016/j.carbpol.2019.115663
34. Mihiretu GT, Chimphango AF, Görgens JF (2019) Steam explosion pre-treatment of alkali-impregnated lignocelluloses for hemicelluloses extraction and improved digestibility. Bioresour Technol 294:122121. https://doi.org/10.1016/j.biortech.2019.122121
35. Isogai A, Usuda M, Kato T, Uryu T, Atalla RH (1989) Solid-state CP/MAS carbon-13 NMR study of cellulose polymorphs. Macromolecules 22(7):3168–3172. https://doi.org/10.1021/ma00197a045
36. Xu F, Shi Y-C, Wang D (2013) X-ray scattering studies of lignocellulosic biomass: a review. Carbohydr Polym 94(2):904–917. https://doi.org/10.1016/j.carbpol.2013.02.008
37. Malaspina DC, Faraudo J (2019) Molecular insight into the wetting behavior and amphiphilic character of cellulose nanocrystals. Adv Colloid Interface Sci 267:15–25. https://doi.org/10.1016/j.cis.2019.02.003
38. Varma AJ, Chavan VB (1995) A study of crystallinity changes in oxidised celluloses. Polym Degrad Stabil 49(2):245–250. https://doi.org/10.1016/0141-3910(95)87006-7
39. Kim U-J, Kuga S, Wada M, Okano T, Kondo T (2000) Periodate oxidation of crystalline cellulose. Biomacromolecules 1(3):488–492. https://doi.org/10.1021/bm0000337
40. Kassaye S, Pant KK, Jain S (2016) Synergistic effect of ionic liquid and dilute sulphuric acid in the hydrolysis of microcrystalline cellulose. Fuel Process Technol 148:289–294. https://doi.org/10.1016/j.fuproc.2015.12.032
41. Johar N, Ahmad I, Dufresne A (2012) Extraction, preparation and characterization of cellulose fibres and nanocrystals from rice husk. Ind Crops Prod 37(1):93–99. https://doi.org/10.1016/j.indcrop.2011.12.016
42. Xiang LY, Mohammed MAP, Samsu Baharuddin A (2016) Characterisation of microcrystalline cellulose from oil palm fibres for food applications. Carbohydr Polym 148:11–20. https://doi.org/10.1016/j.carbpol.2016.04.055
43. Naduparambath S, Jinitha TV, Shaniba V, Sreejith MP, Balan AK, Purushothaman E (2018) Isolation and characterisation of cellulose nanocrystals from sago seed shells. Carbohydr Polym 180:13–20. https://doi.org/10.1016/j.carbpol.2017.09.088
44. Barczyński P, Komasa A, Ratajczak-Sitarz M, Katrusiak A, Dega-Szafran Z, Szafran M (2011) Structure of 3,4-dicarboxy-1-methylpyridinium inner salt studied by X-ray diffraction, DFT calculations, FTIR, Raman and NMR spectra. J Mol Struct 994(1):216–222. https://doi.org/10.1016/j.molstruc.2011.03.021
45. Conley K, Whitehead MA, van de Ven TGM (2016) Chemically peeling layers of cellulose nanocrystals by periodate and chlorite oxidation. Cellulose 23(3):1553–1563. https://doi.org/10.1007/s10570-016-0922-1
46. Serra A, González I, Oliver-Ortega H, Tarrès Q, Delgado-Aguilar M, Mutjé P (2017) Reducing the amount of catalyst in TEMPO-oxidized cellulose nanofibers: effect on properties and cost. Polymers 9(11). https://doi.org/10.3390/polym9110557

47. Querejeta-Fernández A, Chauve G, Methot M, Bouchard J, Kumacheva E (2014) Chiral plasmonic films formed by gold nanorods and cellulose nanocrystals. J Am Chem Soc 136(12):4788–4793. https://doi.org/10.1021/ja501642p
48. de Faria AF, Perreault F, Shaulsky E, Arias Chavez LH, Elimelech M (2015) Antimicrobial electrospun biopolymer nanofiber mats functionalized with graphene oxide–silver nanocomposites. ACS Appl Mater Interfaces 7(23):12751–12759. https://doi.org/10.1021/acsami.5b01639